MULTIPHYSICS SIMULATION OF PV MODULES

Pankaj Arora
pankaj.arora@tecnico.ulisboa.pt
Instituto Superior Técnico, Universidade de Lisboa, Portugal
October 2016

Abstract- Modeling and simulation of Photovoltaic (PV) modules play an important role for the development of the technology and evaluation of new designs. A Finite Element Method (FEM) based multiphysics simulation software is used in this work to study and analyze optical and thermal performance of PV modules. An increase in transmittance at low elevation angles (increase of 10-15% at an elevation angle of 15°) is calculated from simulations of structured glass models. A novel thermal model based on the optical properties of module components is presented to determine the temperature distribution in a PV module. Electrical (ohmic) loss in the emitter for homogeneous and inhomogeneous cell illumination is studied. Using coupled optical and electrical simulations, performance of grid models is investigated. Validation of the multiphysics study is done by outdoor experiments. Experiment and simulation results lay within an average absolute temperature difference of 0.6 ± 2ºC for three different illumination cases investigated.

Keywords- Photovoltaic modules; Finite Element Method; Multiphysics simulation; Structured glass

1. INTRODUCTION

Like most real world systems, PV modules are subjected to a multitude of physical phenomena. Most numerical studies conducted on PV modules found in literature, focus on one of the underlying physics phenomenon. With the help of new FEM software and High Performance Computing (HPC) systems, it is possible to study coupled multiphysical problems accurately. In this paper, multiphysics studies comprising of a combination of ray-tracing, heat transfer and electric current tools are conducted on PV module using the FEM based software COMSOL Multiphysics®. Additionally, the different tools are also independently used to investigate the performance of models proposed in this work.

Reflection losses in fixed (non-tracking) PV installations increase for lower elevation angles. In a study, (Sjerps-Koomen, et al., 1996) [1] , found that for vertically mounted PV modules near the equator, yearly reflection losses due to lower elevation angles relative to Standard Test Conditions (STC) can be as high as 8%.

In order to reduce reflection losses in PV modules, glass structuring has been proposed by various authors (Duell and Ebert, 2010 [2]; Nositschka, 2008 [3]; Krauter, 1993 [4]). Structuring a glass surface prevents the reflected light to be completely lost by directing it to the neighboring surfaces, where it again undergoes reflection and refraction. Pyramid-structured glass models are simulated in this study using a ray-tracing tool based on Fresnel equations and Beer-Lambert law.

The solar energy absorbed by PV cells is converted into electric and thermal energy. Due to the thermal energy absorbed by cell, operating temperature of the solar cells increases. Since, the efficiency of the PV solar cells is inversely proportional to the cell temperature (Green, 1982) [5], it is important to determine the temperature distribution of the PV module. Zhou, et al., 2015 [6]; Siddiqui, et al., 2012 [7]; Lee, Y., et. al. 2012 [8] have conducted studies to simulate and analyze the temperature distribution in PV modules in the past.

All of these studies determine the heat absorbed in the different module components based on constant values of optical coefficients (reflectance, transmittance and absorbance). These coefficients however vary significantly with the irradiance incidence angle. In the model presented, absorption of solar energy in the materials is measured with the help of optical study, which allows analysis for any incidence angle. The attenuation in energy of solar rays as they are absorbed in the different materials is calculated from the optical study. Thus using a multiphysics simulation, heat absorbed in the module can be accurately calculated and used as input for thermal study of PV modules.

The electrical simulation in this thesis calculates the electric (ohmic) losses occurring in the emitter layer of the solar cell. In certain PV systems such as bifacial PV modules, concentrated PV, the cell illumination is inhomogeneous (Johnston, 1998) [9]. Due to this inhomogeneity in illumination, the magnitude of current generated is also non-uniform over cell surface. Thus in order to keep the electrical losses down, a non-uniformly distributed metal grid for inhomogeneous cell irradiance is modeled and studied using FEM based electrical simulation. The electrical simulation is coupled with the optical tool to compute the performance of the proposed grid.

The last section details a multiphysics study, where one-cell PV module is modeled for different illumination patterns. Solar energy absorbed by the different module components results in heating the module, thereby developing a temperature distribution which depends on the absorbed energy. Accuracy of FEM multiphysics simulations in studying real world systems is verified in this part by comparing the simulation results to results of outdoor experiments.

2. OPTICAL SIMULATIONS

2.1 Basic theory and governing equations

The underlying principle of optical simulations is based on ray optics. For a light ray incident on an interface between two optically different media as shown in figure 1, the reflection coefficients are given by Fresnel Equations (eq. 1-5).

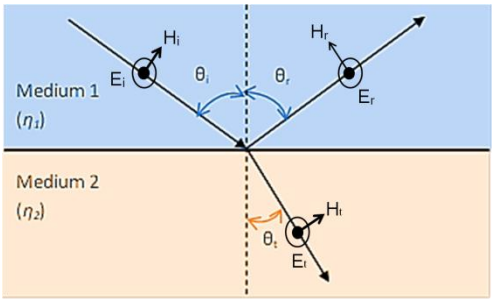

Figure 1: Reflection and refraction of light on a plane surface when an incident ray strikes an interface between two media of different refractive indices

The reflection coefficients depend on the polarization of the light ray. The polarization components can be decomposed into S-type (electric field of the incident ray perpendicular to the plane of incidence - plane containing the incident, reflected, and refracted rays) and P-type (electric field of the incident ray parallel to the plane of incidence). For P-polarized and S-polarized light ray, the reflection power coefficients are given by eq. 3 and eq. 4 (Saleh, et al.,1991 [10]; Born, et al., 2003 [11]).

$$r_p = \frac{n_1 \cos\theta_t - n_2 \cos\theta_i}{n_1 \cos\theta_t + n_2 \cos\theta_i} \quad (1)$$

$$r_s = \frac{n_1 \cos\theta_i - n_2 \cos\theta_t}{n_1 \cos\theta_i + n_2 \cos\theta_t} \quad (2)$$

$$R_p = |r_p|^2 \quad (3)$$

$$R_s = |r_s|^2 \quad (4)$$

where the power coefficients are given by R_p and R_s, n_1 and n_2 are the refractive indices of the media, θ_i and θ_t are the incidence and refraction angles respectively

For unpolarized light rays, the reflection power coefficient, R is given by the average of P-polarized and S-polarized light rays (eq. 5). (Saleh, et al., 1991)

$$R = \frac{1}{2}(R_s + R_p) \quad (5)$$

For an absorbing medium the effective refractive index, is given by eq. 6 [11]:

$$N = n + ik \quad (6)$$

where the effective refractive index of an absorbing medium N consists of real part n, which gives the ratio of the speed of light in free space to the phase velocity of light in the medium and imaginary part k, which determines the absorption by the medium and is called extinction coefficient.

Intensity of rays passing through the medium attenuates depending on the absorption coefficient of the medium defined by eq. 7 (Duffie, et al, 2006) [12].

$$\alpha = \frac{4\pi k}{\lambda} \quad (7)$$

where α is the absorption coefficient, λ is the wavelength of light ray, and k is the extinction coefficient of the medium.

Intensity of a light ray after undergoing reflection at the media interface and absorption in the medium is given by eq. 8 [12].

$$I = I_0\,(1 - R)\,exp\,(-\frac{\alpha d}{\cos\theta_t}) \quad (8)$$

where I is the light intensity at the depth, d of the absorbing material, I_0 is the intensity of light incident on the interface of the media, α is the absorption coefficient of the material, θ_t is the angle of refraction and R is the reflection coefficient given by eq. 5.

The accuracy of the ray-tracing tool of COMSOL was first tested on a simple model of a flat glass which can be evaluated analytically. The glass used in the simulation namely low-iron soda lime glass has almost uniform transmittance (Rubin, 1985) [13] over the spectral range of a silicon solar cells (350 nm to 1.1 µm). The optical study is thus conducted for one particular wavelength of 750 nm to minimize the computational time and resources. Depiction of the different angles mentioned in the paper is shown in figure 2.

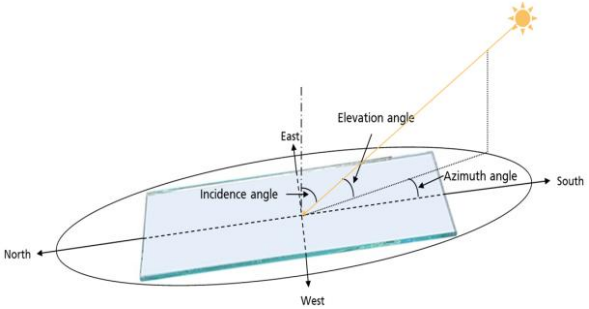

Figure 2: Incidence, elevation and azimuth angles

The simulation results are compared with the theoretically calculated transmittance values which are obtained from equations (1-8) and plotted in figure 3.

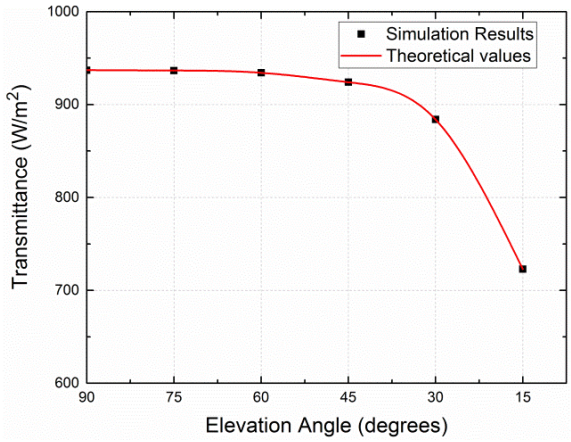

Figure 3: Graph showing transmitted intensity of incident rays at different angles

For all angles considered in the study, the error between the values is less than 0.01%. This good accuracy allows using the ray-tracing tool for complex designs.

2.2 Optical study of structured glass models

Due to an increase in the intensity of the reflected ray (Fresnel's equations), the transmittance at lower elevation angles decreases; this can be seen in figure 3. This lowers the efficiency of the PV module when rays fall on it at lower elevation angles. This is typically the case for photovoltaic applications that are fixed and cannot orient according to position of the sun. PV systems installed on roofs, walls of buildings, streets and pathways are a few of such applications. In order to reduce the optical losses in PV modules (Duell and Ebert, 2010 [2]; Nositschka, 2008 [3]), effective design of the glass (structuring) can be applied.

To enhance the performance of glass at lower elevation angles five structured models are developed and studied. Exemplary model type 5 and its simulation results are presented here in detail.

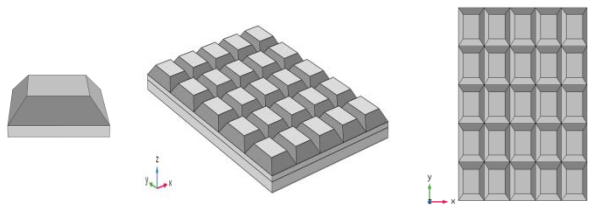

Figure 4: Type 5 structured glass model: surface area of pyramid plateau is 40% of the base

For strength and stability of the modules, each model has a base glass of 2 mm thickness beneath the pyramid-like structures (minimum thickness of solar glass available in the market). Unlike flat glass, transmittance of structured models depends on azimuth angle which is varied in the simulations from 0 to 180 degrees in steps of 30 degrees.

The simulation results showing relative transmission intensity (Incidence Angle Modifier (IAM)) of the glass model type 5 for the different elevation and azimuth angles are depicted in figure 5. To compare the different angular behavior of the structures the transmitted energy is normalized to the normal incidence value.

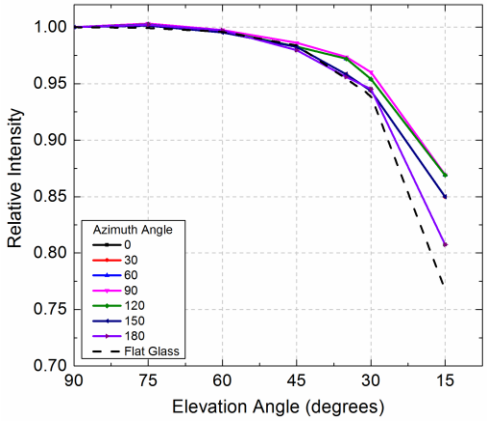

Figure 5: Transmittance computed in Type 5 model at different elevation and azimuth angles and its comparison to transmission through flat glass

From figure 5, we see that at greater elevation angles transmittance of flat and proposed glass model are nearly the same, however as the elevation angle decreases, a substantial improvement is noticed with structured glass. At an elevation angle of 15º, for example, transmittance of the structured glass model at different azimuth angles is higher by 10-15% when compared to flat glass.

The irradiance pattern at the base of type 5 glass model obtained from simulations is shown in figure 6 for (a) elevation angle 90º, azimuth angle 0º, (b) elevation angle 30º, and azimuth angle 30º.

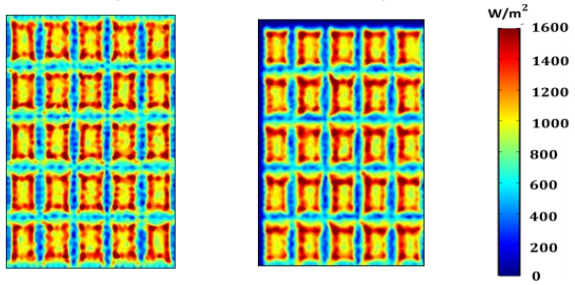

Figure 6: Irradiance profile at the base of type 5 glass model obtained from simulations for (a) elevation angle 90^0, azimuth angle 0^0, (b) elevation angle 30^0, and azimuth angle 30^0

In conclusion, by using the ray-tracing tool of COMSOL multiphysics novel designs can be evaluated before the manufacturing stage. Coupling and simulating several such physics tools for a model of a real system can help provide an accurate understanding of the system.

3 THERMAL SIMULATIONS

3.1 *Basic theory and governing equations*

Solar energy absorbed by the PV cells which is not converted into electrical energy is released in the form of thermal energy. The cell, thus acts as a heat source. The operating temperature of a cell is reached when equilibrium is established between the heat generated by the solar cell and heat lost to the surrounding via convection and radiation.

Heat is transferred within the module components by conduction. Thermal energy in the module is lost to the surroundings by convection and radiation. Governing equation for heat transfer in PV modules can be expressed by equation 2.24 (Sundén, 2012) [14]

$$q_u = q_{cond} - (q_{rad} + q_{conv}) \tag{9}$$

where q_u is the useful energy absorbed by the solar cell, q_{cond}, q_{rad}, q_{conv} are the conductive, radiative and convective heat flux respectively. q_{cond} is given by eq. 10 (Fourier Law)

$$q_{cond} = -k\nabla T \tag{10}$$

where k is the thermal conductivity, and ∇T is the temperature difference between the contact bodies.

q_{rad} is the radiative heat flux given by eq. 11 (Stefan-Boltzmann Law)

$$q_{rad} = \varepsilon\sigma(T^4 - T_{amb}^4) \tag{11}$$

where ε is the emissivity of the surface, σ is the Stefan-Boltzmann constant, T is the temperature of the radiating surface, and T_{amb} is the ambient temperature. This relation for radiative heat transfer holds true if the temperature around the PV modules can be considered equal to the ambient temperature.

q_{conv} is the convective heat flux given by eq. 12 (Newton's law of cooling)

$$q_{conv} = h(T - T_{amb}) \tag{12}$$

where h is the convective heat transfer coefficient given by eq. 13 (Notton, et al., 2005) [15]

$$h = 5.82 + 4.07\,v \tag{13}$$

where v is the wind speed (in meters per second).

3.2 *Thermal study of a one-cell PV module*

A one-cell PV module shown in figure 7 is simulated in this work to calculate the temperature distribution in the PV-module. The temperature distribution is determined from the amount of heat absorbed in each module component, which is obtained from an optical study of the model. To simplify the model, metallization is not considered in the study.

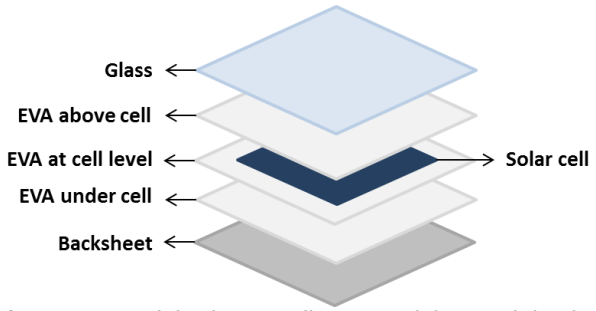

Figure 7: Model of a 1-cell PV module used in the simulations (components are not according to scale)

3.2.1 Assumptions of the simulations

The assumptions considered in the coupled optical and thermal simulations are shown in table 1.

Parameters	Values
Intensity of rays	1000 W/m^2
Wavelength of rays	750 nm
Elevation angle	90 degrees
Ambient Temperature	293.15 K
Wind velocity	1 m/s
Front surface convective coefficient	9.89 Wm^{-2}K^{-1}
Rear surface convective coefficient	4.95 Wm^{-2}K^{-1}

Table 1: Assumptions considered in the simulations

The top and back surface of the PV module is assumed to face the sky and ground respectively. Schott, 1985 [16], found that the sky and ground temperatures can be assumed to be equal to the ambient temperature. The rear surface of the PV module is usually not as efficiently cooled as the front surface, hence the convective heat transfer of the rear surface is considered half that of the front surface (Lee, Y., et. al. 2012) [8].

Material properties of glass, EVA, cell and backsheet are given in Table 2.

	Glass	EVA	Solar cell	Backsheet
Refractive Index, n	1.52 [13]	1.49 [17]	3.72 [18]	1.46 [19]
Extinction coefficient, k	4.07E-7 [13]	1.34E-7 [17]	7.76E-3 [18]	2.98E-7 [20]
Thermal Conductivity (W/m K) **[6]**	2.00	0.311	130	0.15
Specific Heat Capacity (J/kg K) **[6]**	500	2090	677	1250
Density (kg m^{-3}) **[6]**	2450	950	2330	1200
Emissivity **[6]**	0.85	-	-	0.9

Table 2: Material properties of the components used in the simulations

3.2.2 *Results and discussion*

Heat absorbed in the different components calculated from the optical study is shown in table 3.

Material	Heat Absorbed (kW/m^3)
Glass	9.14
EVA above cell	5.21
Cell	4670
EVA at cell level	7.57
EVA under cell	2.96
Backsheet	2.80

Table 3: Heat absorbed in each material of the PV module according to the FEM-model

Absorption of solar energy by the cell increases its temperature which decreases the electrical efficiency of PV modules. The efficiency relation is given by eq. 14 [21].

$$\eta = \eta_{ref}[1 - \beta(T_c - T_{ref})] \quad (14)$$

where electrical efficiency, η_{ref} of the cell at a reference temperature, T_{ref} of 298.15 K is assumed to be 18%, temperature coefficient, β is 0.0045 K^{-1} for PV silicon cells (Zondag, 2008) [22] and T_c is the cell temperature.

The thermal study is iterated based on eq. 14 until the efficiency and the cell temperature converges. The temperature distribution in the thickness of the PV module is shown in figure 8. The results show that the highest temperature of the cell is 328 K, and is located at the center of the module. Due to increase in the cell temperature the electrical efficiency decreases and is calculated to be 15.57%.

The effect of changes in material or boundary conditions (elevation angle, ambient temperature, wind speed, etc) on the system can easily be evaluated with the presented model as compared to the earlier model [6] [7] [8].

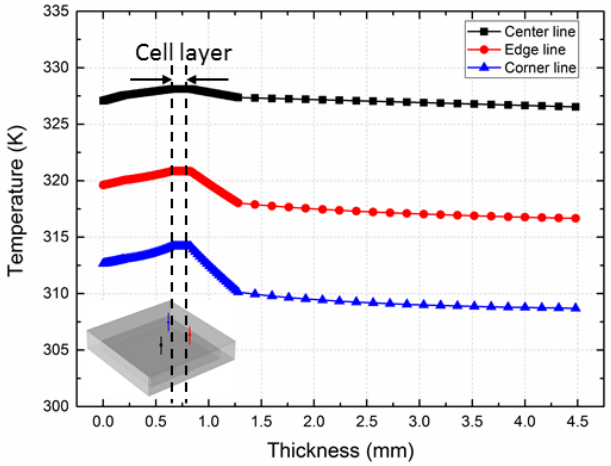

Figure 8: Temperature distribution in the thickness of the PV module at different points

4 ELECTRICAL SIMULATIONS

Current generated in the solar cell pass from the rear surface, vertically through the bulk to the emitter where it flows laterally into the finger, from the finger to the busbar and finally into the interconnecting ribbon from the busbar (Franklin, et al., 2002) [23]. The total series resistance of the cell is given by the sum of all the individual component resistances. Power losses in contact resistances and base resistance are typically much smaller than those in the emitter and metallization (Haas, et al., 2014) [24] and thus have been neglected for the simulations in this work. A significant power loss and reduction in open-circuit voltage due to the thin sheet resistance emitter layer is reported by many studies *(*Smirnov, et al., 1980 [25]; Mitchell, 1977 [26]; Franklin, et al., 2002 [23]*)*. A non-uniform illumination augments the loss [24].

4.1 *Emitter power loss*

Electric loss (dP_{em}) in an infinitesimally small section dx of the emitter surface, shown in figure 9 is given by eq. 15

$$dP_{em} = I^2 dR_e \quad (15)$$

where the differential resistance, dR_e is given by eq 16

$$dR_e = \rho_e \frac{dx}{l} \quad (16)$$

where ρ_e is the emitter sheet resistivity in Ω/square, and l is the finger length given by the distance between the finger edge and busbar as shown in the figure 9.

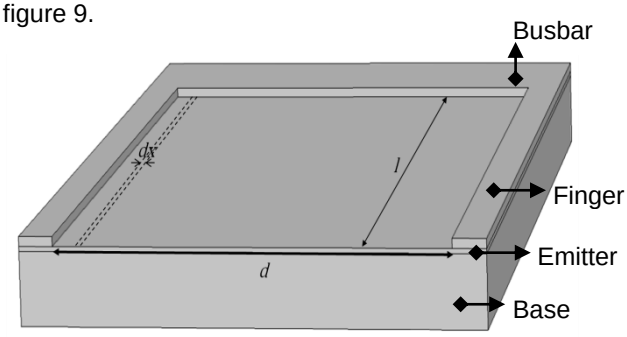

Figure 9: Solar cell cross-section

Under uniform illumination, the lateral current flow, $I(x)$ in the emitter is a spatial function given by eq. 17; its magnitude linearly increasing from zero at the center of the distance to its adjacent fingers to a maximum value at the finger boundary.

$$I(x) = J.l.x \quad (17)$$

where J is the current density due to the illumination.

The total power loss, P_{em} in the emitter region due to lateral current flow in the model shown in figure 9 can be obtained by integrating eq. 15 over the entire surface

$$P_{em} = \int_{-d/2}^{d/2} I^2 \, dR_e = 2 \int_{0}^{d/2} J^2 \, l \, x^2 \rho_e dx = \frac{1}{12} J^2 l \, \rho_e {d_f}^3 \quad (18)$$

where d_f is the distance between adjacent fingers.

The accuracy of the simulation tool is evaluated for a simple cell cross-section shown in figure 9.

4.1.1 Assumptions of the simulations

To carry out the FEM electrical study, the materials are considered to be homogeneous and the material properties independent of temperature.

Parameters	Values
Emitter sheet resistivity, ρ_e	71 Ω/sq (Fellmeth, et al., 2014) [27]
Current density, J	35 mA/cm^2 (Kim H., et al., 2013) [28]

Table 4: Assumptions considered in the simulations

The emitter region is assumed to be uniformly doped. Irradiance is assumed to be uniform and same for the different simulation cases.

4.1.2 Simulation results

The model shown in figure 9 is simulated to compute power loss in the emitter for different finger spacing (d_f). The results are cumulated in table 5:

Finger spacing d_f (mm)	Simulation result (mW)	Analytical value (mW)	Error (%)
1	1.89*10^{-2}	1.89*10^{-2}	**0.32**
1.25	3.69*10^{-2}	3.68*10^{-2}	**0.24**
1.5	6.37*10^{-2}	6.36*10^{-2}	**0.20**
1.75	1.01*10^{-1}	1.01*10^{-1}	**0.18**
2	1.51*10^{-1}	1.51*10^{-1}	**0.14**

Table 5: Comparison of simulation results and analytical solutions

The power loss in emitter computed from the simulations shown in Table 5 is in agreement with the solutions obtained from eq. 18 (error between the values is less than 0.32%). The accuracy of the simulation results compared to the analytical solutions in the case of a simple model with homogeneous illumination allows using a similar approach to perform simulations with inhomogeneous illuminations which are difficult to analyze analytically.

For a homogeneous illumination, emitter loss can be easily calculated using the relation derived above. However, for an inhomogeneous illumination, where the current density can no longer be represented by the relation 17, it is difficult to calculate the power loss by analytical methods. With the help of FEM simulations, electrical loss in an inhomogeneous irradiated cell can be computed as the surface is discretized into fine elements. The performance of metal grid with non-uniform spacing between adjacent fingers is analyzed. The finger spacing at a cell position depends on the cell illumination at that position. Regions with higher irradiance are modeled to have closely spaced fingers. The effect of a modified grid is studied and the results are compared to a cell with a conventional metal grid.

The irradiance of a cell (without metallization) in a structured glass module (type 5) calculated earlier for an elevation angle of 90º with the help of optical simulation is shown in figure 10.

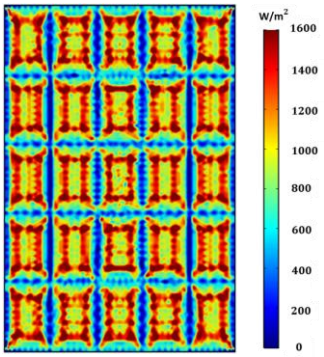

Figure 10: Optical simulation result showing irradiance of a cell in a type 5 structured glass module for an elevation angle of 90º

With the help of the legend of the simulation result, we can see that the irradiance in cell parts under flat pyramid areas is higher than the irradiance in the parts under the pyramid grooves. In this section, the effect of placing the fingers closely in the higher illumination region on both emitter power loss and shading loss is studied with the help of combined optical and electrical simulations. Thus, a coupled optical and electrical study is carried out here to test and optimize a new design.

Two different finger spacing are used to create the grid; a smaller spacing between fingers is used in higher illuminated regions that are under the flat plateau area of the pyramids. To compare the model, another grid with an equal number of fingers but with fingers uniformly distributed over the cell is also simulated. The two finger grid models evaluated are shown in figure 11.

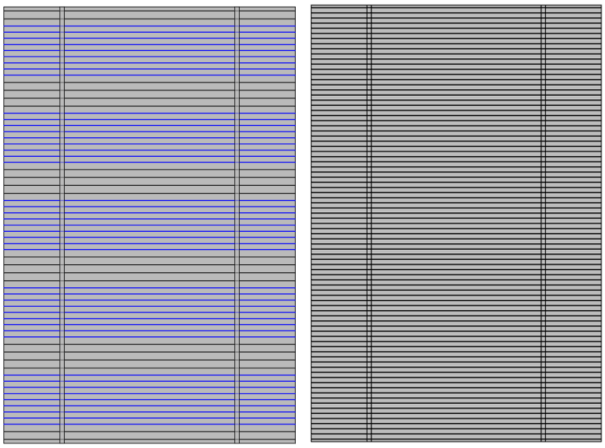

(a) non-uniform finger grid (b) uniform finger grid

Figure 11: Cells with type 5 structured-glass modules **(a)** non-uniform finger grid **(b)** uniform finger grid. Closely spaced fingers are represented in blue color in the non-uniform grid.

First an optical study of the two models is carried out to generate the cell irradiance profile. Due to different arrangement of fingers in the two models the irradiance also differs. The cell irradiance obtained from the optical study of the models is then used in the electrical simulation to calculate the power loss in the emitters. Even though ohmic loss due to emitter resistance only is computed in this work, electrical losses can be calculated for any individual series resistance component or for the entire cell using multiphysics simulations.

The combined optical and electrical simulations give the emitter power loss and average irradiance of the solar cells with the different finger grids and are shown in table 6.

	Emitter power loss (mW)	Average irradiance (W/m^2)
non-uniform finger grid	3.78	880.94
uniform finger grid	3.90	881.37
Relative difference	**3.17%**	**0.05%**

Table 6: Simulation results showing the emitter power loss and average irradiance in the two models studied

Emitter power loss and average irradiance of the solar cell with a non-uniform finger grid is marginally lower than that for the cell with uniform grid. Effect of a lower irradiance due to higher finger shadow loss in the modified grid reduces the improvement attained by a reduction in the emitter power loss. Therefore for structured-glass modules which have inhomogeneous illumination, the low power gain would not legitimate potential higher production costs for custom metallization.

5 EXPERIMENTAL VERIFICATION

This section details the multiphysics study and outdoor experiments carried out on one-cell PV module. Since most part of the thesis is based on simulations, it is important to demonstrate their accuracy in modeling real world situations.

5.1 Experimental set-up

The experiments were conducted outdoors at Fraunhofer ISE, Freiburg with the objective of generating thermal profile on the solar cell with different illumination patterns. To create the illumination patterns on the solar cell, three different masks, shown in figure 12, were employed. The masks have different shaped openings to let solar rays pass through to the cell.

Figure 12: Masks used in the experiments to create different illumination patterns on the cell

All the solar energy absorbed by the cell is converted into thermal energy as the cell is in open circuit mode. Since a thermal profile of the solar cell is desired which is measured with an Infrared (IR) camera, the rear (or non-sunny) side of the solar cell is not covered with EVA or backsheet layers. The experimental set-up is shown in figure 13. The IR camera used is set to capture the temperature profile of the rear side of the solar cell repeatedly at a frequency of 1 second. The IR camera used has an accuracy of ± 2ºC for temperatures below 100 ºC [29].

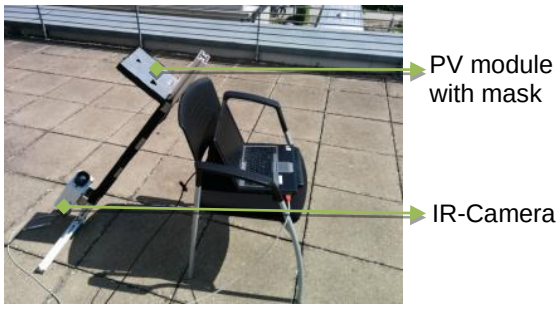

Figure 13: Experimental set-up: a mask is kept in front of the module to create the desired illumination pattern on the solar cell

5.2 Experiment results

The experimentally observed temperature profile of the solar cell back surface for exemplary mask 1 is shown in figure 14.

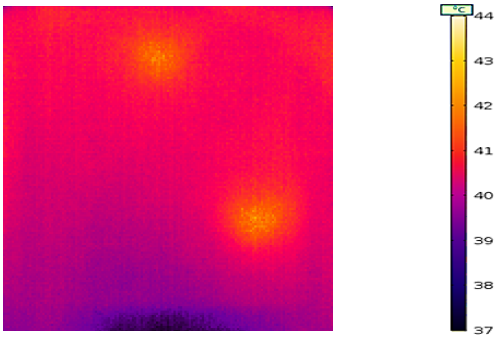

Figure 14: Experimental results showing the temperature profile of the solar cell rear surface for the mask 1

5.3 Multiphysics simulation

The experiment conducted on the module involves coupling of two physical processes, namely:

- Absorption of solar energy in the module,
- Heat exchange from the module.

This experiment is now modeled in the FEM software to assess the accuracy of the simulations. Multiphysics study comprising 'Ray Optics' and 'Heat Transfer' physics tools are used in the simulations to represent the above mentioned processes. The energy absorbed by the components is determined from the optical simulation and is used as input for the thermal study.

5.3.1 Assumptions of the simulation

There are various factors that have to be accounted for in order to represent a real system as a computer model. It is extremely difficult to accurately predict the values of some of these factors. Taking appropriate assumptions in the simulation can reduce the complexity while producing fairly accurate results.

The assumptions considered for the simulation are:

- All the media are homogeneous and have a uniform refractive index.
- The top surface of the PV module is assumed to face the mask whereas the back surface is assumed to face the ground. The ground temperature is assumed to be equal to the ambient temperature [16].
- The ambient conditions are taken to be constant during the experimentation.
- The aluminum beam profile is placed in such a way that the elevation angle of the solar cell is close to 90º.

The assumptions that are imposed on the model in this simulation are defined in table 7.

Parameters	Values
Global Horizontal Irradiance (GHI)[1]	810 W/m^2
Direct Normal Irradiance (DNI)[1]	740 W/m^2
Mean ambient temperature[1]	32.3 ^{0}C
Mean wind velocity[1]	0.71 m/s
Emissivity of glass	0.85
Emissivity of back surface	0.95
Front surface convective coefficient	5.82 Wm^{-2}K^{-1}
Rear surface convective coefficient	8.71 Wm^{-2}K^{-1}
Metal coverage area	0.07% of cell area

Table 7: Assumptions for the FEM multiphysics simulations

[1] Conditions at Freiburg, Germany on 16th August, 2016 at the time experiments were conducted. Values are obtained from Fraunhofer ISE's official weather station.

5.3.2 Simulation results

The simulation results and its comparison to experimental results for mask 1 are shown in figure 15 and table 8.

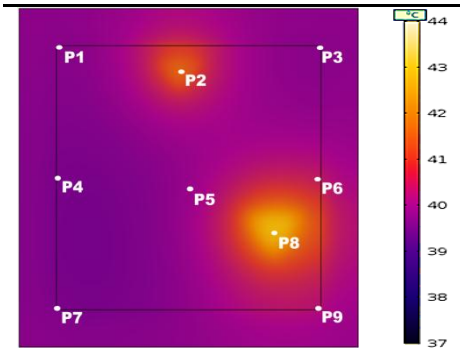

Figure 15: Simulation results showing the temperature profile of the solar cell rear surface for mask 1

Point	Experiment result (ºC)	Simulation result (ºC)	Absolute difference (ºC)
P1	40.7±2	39.6	1.1±2
P2	41.8±2	41.6	0.2±2
P3	40.8±2	39.7	1.1±2
P4	40.2±2	39.5	0.7±2
P5	40.2±2	39.8	0.4±2
P6	40.7±2	40.0	0.7±2
P7	39.5±2	39.5	0.0±2
P8	42.1±2	42.8	0.7±2
P9	39.7±2	40.3	0.6±2
Average over points	40.6±2	40.3	0.6±2

Table 8: Comparison of temperature between experiment and simulation results at points indicated in figure 15 for mask 1

The temperatures at same points in the IR-camera images and in the simulation results for mask 1 demonstrate a high degree of correlation between the experiment and the multiphysics study. The average absolute temperature difference between experimental and simulation results is found to be 0.6±2ºC.

6 CONCLUSIONS

The application of FEM simulations to study PV modules using COMSOL Multiphysics® software is presented in this work. In the first part the ray tracing tool is used to simulate the transmittance of a simple flat glass slab, which can be easily calculated analytically. A maximum error of 0.01% between the simulation results and the theoretical values demonstrate the exactness of the tool, which is then used to simulate complex models designed to improve the transmittance of glass. At lower elevation angles, the proposed pyramid-structured glass models were seen to have 10-15% higher transmittance when compared to flat glass.

In the second part, a new simulation model to analyze thermal behavior of PV modules is presented. In this model the heat absorbed in the different module components is obtained from the optical study. This multiphysics analysis enables fast and accurate assessment of new prototypes.

In order to reduce ohmic losses in the emitter for an inhomogeneous illuminated solar cell, non-uniformly distributed finger grid is designed and modeled. From the multiphysics simulations one can see that although the emitter power loss is reduced in a non-uniform finger grid, the low power gain would not legitimate potential higher production costs for custom metallization.

In the final part, outdoor experiments are carried out to validate multiphysics simulations. The simulation and experiment are repeated for three different illumination patterns to test the efficacy of FEM multiphysics simulations. For the three study cases considered, the average temperature difference between experimental and simulation results is found to be 0.6±2ºC. Further inter-linking of the various physical phenomena (optical, thermal and electrical) is proposed for future work.

REFERENCES

[1] E. Sjerps-Koomen, E. Alsema and W. Turkenburg, "A simple model for PV module reflection losses under field conditions," *Solar Energy,* vol. 57 , no. 6, pp. 421-432, 1996.

[2] M. Duell, M. Ebert, M. Muller, B. Li, M. Koch, T. Christian, R. Perdichizzi, B. Marion, S. Kurtz and D. Doble, "Impact of structured glass on light transmission, temperature and power of PV modules," in *EUPVSEC*, Valencia, Spain, 2010.

[3] A. Nositschka, "Sun-Light Harvesting with Surface Patterned Glass for Photovoltaics," International Materials Institute for New Functionality in Glass, Pittsburgh, PA, USA, 2008.

[4] S. Krauter, Betriebsmodell der optischen, thermischen und elektrischen Parametern von PV-Modulen, Berlin:

Köster, 1993.

[5] M. Green, Solar Cells: Operating Principles, Technology and System Applications, Englewood Cliffs, NJ: Prentice-Hall, Inc., 1982.

[6] J. Zhou, Q. Yi, Y. Wang and Z. Ye, "Temperature distribution of photovoltaic module based on finite element simulation," vol. 111, no. 97-103, 2015.

[7] M. Usama Siddiqui, A. Arif, L. Kelly and S. Dubowsky, "Three-dimensional thermal modeling of a photovoltaic module under varying conditions," vol. 86, no. 2620-2631, 2012.

[8] Y. Lee and A. Tay, "Finite Element Thermal Analysis of a Solar Photovoltaice Module," vol. 15, no. 413-420, 2012.

[9] G. Johnston, "Focal region measurements of the 20 m2 tiled dish at the Australian National University," *Solar Energy,* vol. 63, no. 2, pp. 117-124, 1998.

[10] B. E. A. Saleh and M. C. Teich, Fundamentals of Photonics, New York: Wiley, 1991.

[11] M. Born and E. Wolf, Principles of Optics, vol. Seventh, Cambridge: University Press, 2003.

[12] J. Duffie and W. A. Beckman, Solar Engineering of Thermal Processes, vol. 3, Wiley, 2006.

[13] M. Rubin, "Optical Properties of Soda-Lime Silica Glasses," *Solar Energy Materials,* vol. 12, no. 4, pp. 275-288, 1985.

[14] B. Sundén, Introduction to Heat Transfer, Southampton, Boston: WIT Press, 2012.

[15] G. Notton, C. Cristofari, M. Mattei and P. Poggi, "Modelling of a double-glass photovoltaic module using finite differences," *Applied Thermal Engineering,* vol. 25, pp. 2854-2877, 2005.

[16] T. Schott, "Operational Temperatures of PV modules," in *Proc. 6th European Photovoltaic Solar Energy Conference*, London, UK, 1985.

[17] K. McIntosh, J. Cotsell, J. Cumpston, A. Norris, N. Powell and B. Ketola, "An optical comparison of silicone and EVA encapsulants for conventional silicon PV modules: A ray-tracing study," in *34th IEEE Photovoltaic Specialists Conference*, Philadelphia, 2009.

[18] M. Green and M. Keevers, "Optical properties of intrinsic silicon at 300 K," in *Progress in Photovoltaics: Research and Applications*, vol. 3, John Wiley & Sons Ltd., 1995.

[19] "DuPont Tedlar PVF General properties," 2014. [Online]. Available: http://www.dupont.com/content/dam/dupont/products-and-services/membranes-and-films/pvf-films/documents/DEC_Tedlar_GeneralProperties.pdf. [Accessed September 2016].

[20] R. French, J. Rodriguez-Parada, M. Yang, R. Derryberry and N. Pfeiffenberger, "Optical Properties of polymeric materials for concentrator photovoltaic systems," *Solar Energy Materials & Solar Cells,* vol. 95, pp. 2077-2086, 2011.

[21] D. Evans, "Simplified method for predicting photovoltaic array output," vol. 27, no. 555-560, 1981.

[22] H. A. Zondag, "Flat-plate PV-Thermal collectors and systems: A review," vol. 12, no. 4, 2008.

[23] E. Franklin and J. Coventry, "Effects of highly non-uniform illumination distribution on electrical performance of solar cells," in *Proceedings of Australia & New Zealand Solar Society*, Canberra, 2002.

[24] A. Haas, J. Wilcox, J. Gray and R. J. Schwartz, "Numerical modeling of loss mechanisms resulting from non-uniform illumination in multijunction concentrator solar cells," *International Journal of Numerical Modelling: Electronic Networks, Devices and Fields,* vol. 27, pp. 282-297, 2014.

[25] G. Smirnov and J. Mahan, "Distributed series resistance in photovoltaic devices: intensity and loading effects," *Solid-State Electronics,* vol. 23, no. 10, pp. 1055-1058, 1980.

[26] K. Mitchell, "Computer analysis of resistance and non-uniform illumination effects on concentrator solar cells," in *International Electron Devices Meeting*, Sandia hboratories, AlbuquerqueN,M 87115, 1977.

[27] T. Fellmeth, F. Clement and D. Biro, "Analytical Modeling of Industrial-Related Silicon Solar Cells," *IEEE Journal of Photovoltaics,* vol. 4, no. 1, pp. 504-513, 2014.

[28] J. K. Kim H., E. Lee, D.-W. Kim, J.-H. Yun and J. Yi, "Effect of the short collection length in silicon microscale wire solar cells," *Applied Physics Letters,* vol. 102, no. 19, 2013.

[29] "VarioCAM Operating Instructions," January 2007. [Online]. Available: http://www.infratec.de/fileadmin/media/IRMT/Handbuecher/InfraTec-Manual-VarioCAM.pdf. [Accessed September 2016].